Published in final edited form as:
Photochem Photobiol. 2010 ; 86(6): 1414–1420.

Efficient Singlet Oxygen Generation by Luminescent 2-(2′-Thienyl)Pyridyl Cyclometalated Platinum(II) Complexes and their Calixarene Derivatives

Siu-Wai Lai[1,*], **Ying Liu**[2], **Dong Zhang**[2], **Bin Wang**[1], **Chun-Nam Lok**[1], **Chi-Ming Che**[1], and **Matthias Selke**[2,*]

[1] Department of Chemistry and Open Laboratory of Chemical Biology of the Institute of Molecular Technology for Drug Discovery and Synthesis, and HKU-CAS Joint Laboratory on New Materials, The University of Hong Kong, Pokfulam Road, Hong Kong SAR, China

[2] Department of Chemistry and Biochemistry, California State University Los Angeles, Los Angeles, California 90032, U. S. A

Abstract

Luminescent cyclometalated platinum(II) complexes, namely $[Pt(Thpy)(PPh_3)X]^{n+}$ (HThpy = 2-(2′-thienyl)pyridine; X = Cl^- (**1**), n = 0; X = CH_3CN (**2**), pyridine (**3**), n = 1) and $[Pt(Thpy)(HThpy)Y]^{n+}$ (Y = Cl^- (**4**), n = 0; Y = pyridine (**5**), n = 1), exhibit structured emission with peak maximum at ~556 and 598 nm in degassed acetonitrile and with emission quantum yield and lifetime of up to 0.38 and 26 μs respectively. These complexes are efficient photosensitizers of singlet oxygen with yields up to > 90%. Complex **5** exhibited photocytotoxicity towards cancer cells and fluorescence microscopic images of cells incubated with **5** reveal substantial uptake at the nucleus and mitochondria.

INTRODUCTION

Photosensitized production of singlet molecular oxygen, $^1O_2$, has been widely investigated for non-radical aerobic oxidation, photodynamic therapy (PDT) and polymer science (1–16). Apart from organic photosensitizers commonly used for the generation of singlet oxygen, transition metal complexes have recently been shown to be attractive alternatives due to their strong absorptions in the UV-visible region, long-lived triplet metal-to-ligand charge transfer (MLCT) states, high emission quantum efficiencies of the triplet state, and high photostability (17–23). In the past decades, Che and coworkers investigated the photoluminescent properties of cyclometalated platinum(II) complexes, namely $[Pt(C\text{^}N\text{^}N)R^1]^{n+}$ bearing tridentate C-deprotonated 6-phenyl-2,2′-bipyridine $[C\text{^}N\text{^}N]^-$ and related ligands (24–27), and $[Pt(Thpy)R^2R^3]^{n+}$ with bidentate Thpy ligand (HThpy = 2-(2′-thienyl)pyridine) (28–30). Their spectroscopic characteristics were reported to vary significantly with the electronic properties and structure of the ancillary ligands ($R^{1–3}$).

Under aerobic conditions, the MLCT excited states of cyclometalated platinum(II) complexes are quenched by triplet dioxygen, which may lead to formation of singlet oxygen

[*]Corresponding author: swlai@hku.hk (Siu-Wai Lai), mselke@calstatela.edu (Matthias Selke).

SUPPLEMENTARY MATERIALS

Additional Supplementary Materials may be found in the online version of this article: Spectroscopic data, crystallographic data, photophysical spectra, and biological studies.

Table S1-3 and Figure S1-8 can be found at DOI: 10.1562/2010-xxxxxx.s1.

in various amounts (20,21). Previous studies have established that the amount of singlet oxygen photosensitized by these complexes depends on the excited state redox potential, and steric bulk of the cyclometalated ligand (20,21). However, other variables may be involved in determining whether or not a late transition cyclometalated complex is capable of producing singlet oxygen in high yield. Despite the fact that the photophysical properties of literally hundreds of cyclometalated complexes have been investigated under anaerobic conditions, there is a surprising paucity of data for their behavior in the presence of dioxygen and light. Thus, the effects of ancillary ligand(s), solvent, neighbouring metal ion(s) (in polynuclear complexes), as well as electronic charge on the metal center have not been investigated towards the production of singlet oxygen in these complexes.

Herein we describe the photophysical properties and production of singlet oxygen from a series of cyclometalated $[Pt(Thpy)(PPh_3)X]^{n+}$ and $[Pt(Thpy)(HThpy)Y]^{n+}$ complexes (**1–5**; Scheme 1). We therefore envisage, through varying the ancillary X or Y group, the emission properties can be systematically modified and probed to maximize the efficiency of $^1O_2$ production. With reference to previous studies on luminescent biological probes based on cyclometalated iridium(III) and platinum(II) complexes with auxiliary ligands modified with amino acids (20,31), we anticipate that the 2-(2′-thienyl)pyridyl platinum(II) complexes which display visible emission with long emission lifetime and high quantum yields for $^1O_2$ production (21), are photosensitizers for the generation of singlet oxygen of biological interest. In addition, the red-shifts in absorption and emission of these new photosensitizers are advantageous towards shifting the operational window of PDT into the tissue transparency window at 700–1100 nm.

We also envision that 2-(2′-thienyl)pyridyl platinum(II) complexes incorporated into upper-rim phosphinated calix[4]arenes, as reported previously by us (30), could be developed as photosensitizing hosts towards target guests. Therefore we describe the production of singlet oxygen by complexes $[(PtThpyCl)_2L]$ (**6**) and $[\{PtThpy(CH_3CN)\}_2L](ClO_4)_2$ (**7**), where L is 5,17-bis(diphenylphosphino)-25,26,27,28-tetra-n-butoxycalix[4]arene. The selectivity of binding would be affected by the moieties at the lower rim of the calixarenes, and/or their conformation and size.

MATERIALS AND METHODS

Materials and General Procedures

[Pt(Thpy)(HThpy)Cl] (**4**) was prepared by the literature method (28–29). Acetonitrile for photophysical measurements was distilled over potassium permanganate and calcium hydride. Dichloromethane for photophysical studies was washed with concentrated sulfuric acid, 10 % sodium hydrogen carbonate, and water, dried by calcium chloride, and distilled over calcium hydride. All other solvents were of analytical grade and purified according to conventional methods (32).

Instrumentation and Physical Measurements

Fast atom bombardment (FAB) mass spectra were obtained on a Finnigan Mat 95 mass spectrometer with a 3-nitrobenzyl alcohol matrix, whereas electrospray mass spectra were obtained on a LCQ quadrupole ion trap mass spectrometer. High-resolution ESI mass spectra were obtained from a Waters Micromass Q-Tof Premier quadrupole time-of-flight tandem mass spectrometer. ^1H (500 MHz), ^{13}C (126 MHz) and ^{31}P (202 MHz) NMR spectra were performed on DPX 500 Bruker FT-NMR spectrometer with chemical shifts (in ppm) relative to tetramethylsilane (^1H and ^{13}C) and H_3PO_4 (^{31}P) as references. Elemental analyses were performed by the Institute of Chemistry at the Chinese Academy of Sciences,

Beijing. UV-vis spectra were recorded on a Perkin Elmer Lambda 19 UV/vis spectrophotometer.

Emission and Lifetime Measurements

Steady-state emission spectra were recorded on a Fluorolog-3 Model FL3-21 spectrophotometer. Solution samples for measurements were degassed with at least four freeze-pump-thaw cycles. Low-temperature (77 K) emission spectra for glassy solutions and solid-state samples were recorded in 5 mm diameter quartz tubes, which were placed in a liquid nitrogen Dewar equipped with quartz windows. The emission spectra were corrected for monochromator and photomultiplier efficiency and for xenon lamp stability. Emission lifetime measurements were performed with a Quanta Ray DCR-3 pulsed Nd:YAG laser system (pulse output 355 nm, 8 ns). The emission signals were detected by a Hamamatsu R928 photomultiplier tube and recorded on a Tektronix TDS 350 oscilloscope. Errors for λ values (±1 nm), τ (±10 %), Φ (±10 %) were estimated.

Luminescence quantum yields were determined using the method of Demas and Crosby (33) with $[Ru(bpy)_3]Cl_2$ in degassed acetonitrile as a standard reference solution ($\Phi_r = 0.062$) and calculated according to the following equation: $\Phi_s = \Phi_r(B_r/B_s)(n_s/n_r)^2(D_s/D_r)$, where the subscripts *s* and *r* refer to sample and reference standard solution respectively, *n* is the refractive index of the solvents, *D* is the integrated intensity, and *Φ* is the luminescence quantum yield. The quantity *B* was calculated by $B = 1 - 10^{-AL}$, where A is the absorbance at the excitation wavelength and L is the optical path length. The UV-visible absorption and emission spectral data of **1–5** are listed in Table S1 (see Supplementary Materials).

Synthesis

Preparation and characterization of $[Pt(Thpy)PPh_3Cl]$ (**1**) and $[Pt(Thpy)PPh_3(CH_3CN)]ClO_4$ (**2**) were documented by us previously (30). Using similar synthetic procedures adapted for **2** except pyridine was used as solvent, $[Pt(Thpy)PPh_3(py)]ClO_4$ (**3**) and [Pt(Thpy)(HThpy)py]ClO_4 (**5**) were obtained by using $[Pt(Thpy)PPh_3Cl]$ (**1**) and [Pt(Thpy)(HThpy)Cl] (**4**) as precursors, respectively.

$[Pt(Thpy)PPh_3(py)]ClO_4$, 3

A mixture of $[Pt(Thpy)PPh_3Cl]$ (**1**) (0.10 g, 0.15 mmol) and $AgClO_4$ (0.04 g, 0.19 mmol) in pyridine (10 mL) stirred at room temperature for 15 min afforded a pale yellow solution and white precipitate of AgCl. The pale yellow solution was separated from the white solid and was centrifuged for 3 min to remove residual AgCl solid. Addition of diethyl ether yielded a yellow solid, which was recrystallized by vapor diffusion of diethyl ether into a CH_2Cl_2/CH_3OH (2:1 v/v) solution of the crude product to afford yellowish orange crystals. Yield: 0.10 g, 82 %. ^{1}H NMR (CD_2Cl_2): *δ* 5.92 (d, *J* = 4.9 Hz, 1H), 6.99–7.06 (m, 3H), 7.30 (t, *J* = 7.0 Hz, 2H), 7.35–7.38 (m, 6H), 7.50 (t, *J* = 7.4 Hz, 3H), 7.58–7.63 (m, 7H), 7.82 (t, *J* = 7.8 Hz, 1H), 7.90 (t, *J* = 7.7 Hz, 1H), 8.38 (d, *J* = 6.4 Hz, 2H). $^{13}C\{^1H\}$ NMR (CD_2Cl_2): *δ* 118.6, 121.6 (d, *J* = 3.4 Hz), 127.4, 127.5, 127.7, 128.0, 128.8 (d, *J* = 11.4 Hz), 131.9 (d, *J* = 2.3 Hz), 134.6 (d, *J* = 11.4 Hz), 135.7 (d, *J* = 4.6 Hz), 139.3 (d, *J* = 8.8 Hz), 139.7, 141.6, 143.2, 146.8, 151.4, 160.7. $^{31}P\{^1H\}$ NMR (CD_3CN): *δ* 19.02 (t, with ^{195}Pt satellites, $^1J_{PtP}$ = 4124 Hz). ESI-MS: *m/z* 696.2 [M^+], 617.1 [M – py]$^+$. Anal. Calcd for $C_{32}H_{26}N_2O_4PSPtCl$: C, 48.28; H, 3.29; N, 3.52. Found: C, 48.42; H, 3.42; N, 3.29 %.

[Pt(Thpy)(HThpy)py]ClO_4, 5

The procedure for synthesis of **3** was applied using [Pt(Thpy)(HThpy)Cl] (**4**) (0.09 g, 0.16 mmol) to yield 0.096 g (85 %) of a yellow orange crystalline solid. ^{1}H NMR (CD_2Cl_2): *δ* 5.33 (s, 1H), 6.35 (d, *J* = 4.8 Hz, 1H), 6.93 (t, *J* = 6.7 Hz, 1H), 7.16 (t, *J* = 4.4 Hz, 1H), 7.31

(d with broad ^{195}Pt satellites, 1H, $^{3}J_{HH}$ = 5.9 Hz), 7.47–7.54 (m, 5H), 7.64 (d, *J* = 5.0 Hz, 1H), 7.68 (d, *J* = 3.7 Hz, 1H), 7.78 (d, *J* = 7.3 Hz, 1H), 7.87 (t, *J* = 7.8 Hz, 1H), 7.95 (t, *J* = 7.8 Hz, 1H), 8.05 (t, *J* = 7.9 Hz, 1H), 8.24 (broad s, 1H), 9.26 (d with broad ^{195}Pt satellites, 1H, $^{3}J_{HH}$ = 5.9 Hz). $^{13}C\{^{1}H\}$ NMR (CD_2Cl_2): δ 118.7, 120.8, 125.5, 127.2, 127.3, 128.2, 129.1, 129.9, 130.4, 130.9, 139.5, 139.7, 139.8, 140.7, 140.8, 142.9, 148.7, 150.8, 154.1, 155.6, 163.2. ESI-MS: *m/z* 595.1 [M^+], 516.1 [M–py]$^+$. Anal. Calcd for $C_{23}H_{18}N_3O_4S_2PtCl$: C, 39.74; H, 2.61; N, 6.05. Found: C, 39.73; H, 2.63; N, 6.09 %.

X-ray Crystallography

Crystals of [Pt(Thpy)PPh_3(CH_3CN)]ClO_4 (**2**) were obtained by vapour diffusion of diethyl ether into an acetonitrile solution of the complex, whereas crystals of [Pt(Thpy)PPh_3(py)]ClO_4•(C_2H_5)$_2$O (**3**•(C_2H_5)$_2$O) and [Pt(Thpy)(HThpy)py]ClO_4 (**5**) were grown by vapour diffusion of diethyl ether into a CH_2Cl_2/CH_3OH (2:1 v/v) solution of the respective complex. The crystal data and details of data collection and refinement are summarized in Table S2 (see Supplementary Materials).

Diffraction data for **2**, **3**•(C_2H_5)$_2$O, and **5** were collected at 301 K on a Bruker Smart CCD 1000 diffractometer using graphite monochromatized Mo-Kα radiation (λ = 0.71073 A). For **3**•(C_2H_5)$_2$O and **5**, raw frame data were integrated with SAINT (34) program and semi-empirical absorption correction with SADABS (35) was applied. The structures were solved by the direct method employing SHELXS-97 (36) program on a PC. Pt, P, S, Cl and many non-H atoms were located according to the direct methods. The positions of other non-hydrogen atoms were found after successful refinement by full-matrix least-squares using the program SHELXL-97 (36) on a PC. For **2**, one crystallographic asymmetric unit consists of one formula unit. One perchlorate anion was also located. The absolute structure was assisted by the Flack absolute structure parameter, which is equal to 0.013(7). For **3**•(C_2H_5)$_2$O, one crystallographic asymmetric unit consists of one formula unit. One perchlorate anion and one diethyl ether solvent molecule located. For **5**, one crystallographic asymmetric unit consists of one formula unit. One perchlorate anion was also located.

Emission Quenching Measurements for Cyclometalated Complexes

Luminescence quenching studies were conducted in dilute solutions (concentration of complexes **1–7** = 1×10^5 M) in acetonitrile or dichloromethane that were purged for five minutes with N_2, air or dioxygen. The concentration of oxygen for samples in air (0.00183 M^{-1}) and dioxygen (0.00868 M^{-1}) was estimated from published oxygen solubility data (37). Samples were excited with a 405 nm pulsed diode laser having a pulse duration of *ca*. 1.2 ns and an energy of 500 nJ pulse^{-1}.

Set-up for Time-Resolved Detection of $^1O_2$ NIR Emission

Singlet oxygen quantum yields and luminescence quenching rates of $^1O_2$ were determined using a time-resolved Nd:YAG laser set-up (Minilase II, New Wave Research Inc., excitation pulse 1 ns) and a liquid N_2 cooled Ge photodetector (Applied Detector Corporation Model 403 S). A Schott color glass filter (model RG850; cut-on 850 nm; Newport, USA) was taped to the sapphire entrance of the detector to block any additional ultraviolet and visible light from entering. The port opening to the detector contained the remaining filters: a long wave pass filter (silicon filter model 10LWF ~ 1000; Newport, USA) which transmits in the range of 1100–2220 nm and blocks in the range of 800–954 nm; a band pass filter (model BP-1270–080-B*; CWL 1270 nm; Spectrogen, USA) which blocks in the UV, visible, and IR regions and only transmits in the range of 1200 to 1310 nm with a maximum transmission of 60% at 1270 nm. Signals were digitized on a LeCroy 9350 CM 500 MHz oscilloscope and analyzed using Origin software. All of those experiments were carried out at ambient temperature under air. A 250 W tungsten lamp (Oriel

Instruments) equipped with a 10 cm H_2O filter and 492 nm cutoff filter was used for steady-state generation of $^1O_2$.

$^1O_2$ Quantum Yield Measurements

Samples were prepared in acetonitrile or dichloromethane with absorbances between 0.1–0.3 at 355 nm or 532 nm excitation wavelengths. The absorbance of the reference sensitizers (C_{60}, perinaphthenone and methylene blue) and the metal complex were matched within 80%. The initial $^1O_2$ intensity was extrapolated to $t = 0$. The data points of the initial 0–5 μs were not used due to electronic interference signals from the detector.

$^1O_2$ Quenching Measurements

The quenching rates of $^1O_2$ were measured by Stern-Volmer analysis using Methylene Blue and C_{60} as external sensitizers in CD_3CN and CD_2Cl_2, respectively. The concentration of the metal complexes used in the measurements ranged between 0.1–10 mM.

Binding Studies on Calf Thymus DNA and Bovine Serum Albumin (BSA)

Calf thymus DNA and bovine serum albumin (BSA) were purchased from Sigma Chemical Co. A 20 mM phosphate buffered saline (PBS) solution of pH 7.2 was prepared by dissolving 1.25 g of Na_2HPO_4, 0.35 g of NaH_2PO_4, and 8.0 g of NaCl in 1 L of doubly distilled water. Complex **5** (1.78×10^{-3} g) was first dissolved in 0.256 mL dimethyl sulfoxide (DMSO) to afford a solution with concentration of 1×10^{-2} M. Dilution of the complex solution in DMSO with Tris buffer solution was achieved to afford the solution with complex concentration of 1×10^{-5} M. The concentration of DMSO in the resultant Tris buffer solution should be ~0.1 %. The emission spectral titrations were carried out on 3-mL solutions of **5** (complex concentration = 1×10^{-5} M) with increasing amounts of calf thymus DNA or BSA to give [DNA]/[Pt] between 3 and 18 and [BSA]/[Pt] between 0.1 and 0.6 respectively. DNA was added in 11 μL increments to the complex solution (1×10^{-5} M) in Tris buffer, whereas BSA was added in 0.3 μL increments to the complex solution (1×10^{-5} M) in PBS solution. The solution was mixed well and was allowed to stand for 5 minutes. The emission spectra were recorded upon each addition of 3 equivalents of DNA or 0.1 equivalent of BSA to the solution of **5**, wherein the dilution of complex concentrations upon addition of DNA or BSA was negligible.

Photocytotoxicity

HeLa cells (Human cervical carcinoma) were seeded in a 96-well flat-bottomed microplate at 1×10^4 cells/well in 100 μL MEM (minimum essential medium) containing 10% fetal bovine serum (FBS) and incubated for 24 h. Complex **5** was dissolved in DMSO as a 1×10^{-2} M stock solution, and subsequently diluted with the medium and added to each well with final concentration of DMSO ≤ 1%. For determination of photocytotoxicity, cells were irradiated at room temperature for 30 min on a translucent plastic platform using broadband visible light (~1 mW/cm^2). After further incubation for 48 h, 10 μL of (3-(4,5-dimethyl-2-thiazoyl)-2,5-diphenyltetrazolium bromide (MTT, 5 mg/mL) was added to each well and incubation was continued for 4 h. 100-μL Solubilization solution (10% SDS in 0.01 M HCl) was added to dissolve the formazan and the absorbance at 550 nm was measured with a microplate reader.

Fluorescence Microscopy

HeLa cells were seeded in 35 nm glass bottom dishes at 2×10^5/dish in 2 mL MEM containing 10% FBS and then incubated for 24 h. Cells were treated with 5 μM of **5** for 1 h and examined with a fluorescence microscope (Zeiss Axiovert 200M and FluoArc) using FITC (fluorescein isothiocyanate) filter. Nucleus and mitochondria were stained with 5 μM

Hoechst 33342 (Invitrogen) and 50 nM MitoTracker Red (Invitrogen), respectively, for 10 min.

RESULTS

Synthesis and characterization of **1**, **2**, and **4** have been reported previously (28–30), whereas complexes **3** and **5** were prepared by similar synthetic procedures as developed for **2**, except pyridine was used as solvent in the reactions using precursors **1** and **4,** respectively. Complexes **3** and **5** were characterized by ^{1}H and $^{13}C\{^{1}H\}$ spectroscopy, ESI mass spectrometry, and X-ray crystallography (see Supplementary Materials). They are air- and moisture-stable at room temperature. We have investigated the UV-visible absorption and emission properties of **1–5**; the spectral data and spectra are given in the Supplementary Materials. The absorption spectra of **1–5** in acetonitrile show high-energy, intense absorption band with λ_{max} at 228–330 nm (ε = 17600–41100 M^{-1} cm^{-1}), which are attributed to spin-allowed intraligand ^{1}IL: π(Thpy) → π^*(Thpy) transitions. The moderately intense, low-energy band with λ_{max} at 389–419 nm (ε = 2400–5600 M^{-1} cm^{-1}) is assigned to a spinallowed metal-to-ligand charge transfer ^{1}MLCT: Pt(5d) → π^*(Thpy) transition (28–30).

The emission spectra of **1–3** in degassed acetonitrile at 298 K exhibit predominantly vibronically structured bands with peak maximum at ~556 and 600 nm and a minor broad peak at λ_{max} = 467 nm. Comparison of the emission data among complexes **1–3** reveals an increase in both of the emission intensity and lifetime upon replacing the coordinated chloride ligand in **1** with the neutral nitrogen donor ligands, namely acetonitrile (in **2**) and pyridine (in **3**), respectively. This ligand modification causes an increase in the cationic charge of the platinum(II) complexes, consequently leading to lowering in energy of the occupied Pt(5d) orbitals. Thus the energy of d-d excited state increases accounting for the increase in emission intensity and lifetime. The low-energy emission bands (λ > 550 nm) show a dramatic decrease in intensity upon exposure to air, while the high-energy peak at 467 nm is insensitive to the exposure to air with no change in the emission intensity (38). Similarly, the emission lifetime at λ_{max} > 550 nm shows substantial diminution upon aeration of the solution. For example, the emission lifetime of [Pt(Thpy)PPh_3(py)]ClO_4 (**3**) in degassed CH_3CN at λ_{max} 556 nm is 6.73 μs, whereas upon exposure to air, the emission lifetime decreases to 0.26 μs. The low-energy emission bands with λ_{max} > 550 nm were previously assigned to triplet excited states with mixed ^{3}MLCT and ^{3}IL character (29,39,40). Therefore, the triplet mixed ^{3}MLCT/^{3}IL emissive excited states of [Pt(Thpy)(PPh_3)X]$^{n+}$ complexes can be efficiently quenched by triplet dioxygen. The emission spectra of **4** and **5** in acetonitrile show low-energy structured bands with peak maxima at ~558 and 602 nm, which can be similarly assigned to having mixed ^{3}MLCT and ^{3}IL parentage.

The quantum yields for singlet oxygen production (Φ_Δ) photosensitized by [Pt(Thpy)(PPh_3)X]$^{n+}$ and [Pt(Thpy)(HThpy)Y]$^{n+}$ complexes were obtained by time-resolved laser measurements of near-infrared luminescence signal (1270 nm) intensity of $^{1}O_2$ as a function of absorption at a 355-nm excitation wavelength in deuterated acetonitrile and dichloromethane (Table 1). Figure 1 depicts a typical linear graph of $^{1}O_2$ emission intensity against absorption of selected sensitizers of **1** and **7** in CD_3CN; the singlet oxygen quantum yields were calculated with reference to methylene blue. Similar plots were obtained in CD_2Cl_2 (see Supplementary Materials) using C_{60} (Φ_Δ = 1) as a reference compound. Triplet-triplet annihilation was negligible at these concentrations, as evidenced by the fact that the $^{1}O_2$ intensity showed a linear correlation with the absorption of the complexes. The values of $^{1}O_2$ quantum yields for complexes **1–7** in CD_3CN range from 0.42 ± 0.03 to 0.95 ± 0.05 as listed in Table 1.

Singlet oxygen quenching by ground-state sensitizer may limit the usefulness of the singlet oxygen sensitizer. We therefore determined the total rate constants (k_T) of $^1O_2$ quenching by the ground state of 2-(2′-thienyl)pyridyl platinum(II) complexes as summarized in Table 1. The second order quenching rate constants were obtained from the slopes of linear least-squares fits to the data. The rate constants of the quenching of $^1O_2$ by **1–7** are in the range of ($9.1 \times 10^6 – 5.56 \times 10^7$) M^{-1} s^{-1}, where relatively higher quenching rate constants were observed from $[Pt(Thpy)(HThpy)Y]^{n+}$ systems (**4** and **5**). The rate constants of singlet oxygen quenching by $[Pt(Thpy)]^+$-modified calixarene receptors (**6** and **7**) were observed to be 9.0×10^6 and 1.70×10^7 M^{-1} s^{-1} respectively, which are comparable to those for their mononuclear congeners, **1** ($k_T = 1.40 \times 10^7$ M^{-1} s^{-1}) and **2** ($k_T = 1.26 \times 10 M^{-1}$ s^{-1}). Overall the values for k_T are quite similar to those of standard organic photosensitizers (e.g. TPP, $k_T = 2 \times 10$ M^{-1} s^{-1}).

To evaluate the potentials of these cyclometalated platinum(II) complexes in photobiology, studies on their cytotoxicity, photocytotoxicity, DNA and protein binding, have been performed. Complexes $[Pt(Thpy)(PPh_3)py]ClO_4$ (**3**) and $[Pt(Thpy)(HThpy)py]ClO_4$ (**5**) with relatively high quantum yields of singlet oxygen production were chosen for cytotoxicity studies towards HeLa cancer cells (human cervical epithelioid carcinoma). The half maximal inhibitory concentration (IC_{50}) of **3** in the dark is 21.07 μM. After exposure to visible light, its cytotoxicity was significantly enhanced with the IC_{50} value decreased to 3.29 μM. Similarly, photocytotoxicity was observed for **5** with the IC_{50} in the dark of 6.12 μM and 1.78 μM after visible light irradiation (Fig. 2).

The emission spectrum of **5** (λ_{ex} = 400 nm; concentration = 1×10^{-5} mol dm^{-3}) in Tris buffer solution at room temperature shows a minor band at 464 nm and a predominant slightly vibronic structured band with peak maxima at 553 and 596 nm. Upon gradual addition of calf thymus DNA (3 equivalents per interval up to 18 equivalents) to a Tris buffer solution of **5**, the emission intensities at both λ_{max} of 464 and 553 nm increase. Similar emission spectral traces of **5** at different equivalents of bovine serum albumin (BSA) were performed in PBS solutions at 298 K (λ_{ex} = 400 nm, concentration = 1×10^{-5} M). With addition of 0.1 equivalent of BSA per interval, the emission at 462 nm shows minute increase in intensity, whereas the lower-energy emission bands are slightly red-shifted to 557 and 601 nm and exhibit enhancement in intensity by ~6 times at 0.6 equivalent of BSA from that before the addition of BSA.

We also examined the cellular uptake and localization of **5** in live cells. Fluorescence microscopic images of HeLa cancer cells after incubation with **5** for 1 h revealed noticeable appearance of discrete intracellular fluorescence signals (Figs. 3a and 4a). Staining of cells with fluorescent probe for nuclear DNA (Hoechst 33342, Fig. 3b) or mitochondria (MitoTracker Red, Fig. 4b), demonstrated that **5** was colocalized to the nucleus as well as to mitochondria.

DISCUSSION

Previous studies on singlet oxygen production by cyclometalated complexes have primarily focused on the nature of the encounter complex between triplet dioxygen and the excited metal complex. In many cases, the excited state redox potential of the metal complex may play a major role in determining how much singlet oxygen is produced (20,21). This study shows that ancillary ligands can also drastically increase the amount of singlet oxygen produced by cyclometalated complexes: the quantum yield of $^1O_2$ production (Φ_Δ) depends on the quantum yield of triplet-state formation. Through comparisons of emission quantum yields (Φ) of complexes **1–7** with their respective $^1O_2$ quantum yields (Φ_Δ), a general trend of increase in Φ_Δ can be obtained with increasing Φ. The $^1O_2$ quantum yields (Φ_Δ) of **1–3**

follow the order of X = Cl^- < CH_3CN ~ pyridine, increasing from (0.44 ± 0.02) in **1** to (0.75 ± 0.04) in **2** and (0.82 ± 0.06) in **3**. Similar observations have been made for **6** and **7**, where the respective Φ_Δ in CD_3CN is enhanced from 0.42 ± 0.03 (**6**) to 0.81 ± 0.06 (**7**), when the Cl^- ligand is changed to CH_3CN. Increasing the strength of Y by changing Cl^- to pyridine in complexes **4** and **5**, formulated as $[Pt(Thpy)(HThpy)Y]^{n+}$, results in a significant increase in the $^1O_2$ quantum yield (Φ_Δ) from 0.56 ± 0.04 (**4**) to 0.95 ± 0.05 (**5**) in CD_3CN. On the other hand, replacing the PPh_3 ligand in $[Pt(Thpy)(PPh_3)Cl]$ (**1**) with the HThpy ligand (Complex **4**, [Pt(Thpy)(HThpy)Cl]) gives only a minor enhancement in Φ_Δ in CD_3CN from 0.44 ± 0.02 (**1**) to 0.56 ± 0.04 (**4**). Similar observations were made for the complexes (**3**) and $[Pt(Thpy)(PPh_3)py]^+$ $[Pt(Thpy)(HThpy)py]^+$ (**5**), where again the two complexes differ from each other by **3** bearing the PPh_3 ligand and **5** having the HThpy ligand. The Φ_Δ of **3** and **5** in CD_3CN are comparable being 0.82 ± 0.06 (**3**) and 0.95 ± 0.05 (**5**), respectively.

Φ_Δ can also be influenced by the solvent; for example, $Pt(Thpy)(HThpy)py]ClO_4$ (**5**) shows substantial variation in Φ_Δ when measured in CD_3CN (0.95 ± 0.05) and CD_2Cl_2 (0.27 ± 0.03). Incidentally, the photoluminescent characteristics of **5** is also solvent sensitive; the high-energy absorption maximum shows a bathochromic shift from λ_{max} at 291 nm (ε = 24200 M^- cm^{-1}) in CH_2Cl_2 to 305 nm (ε = 24100 M^- cm^{-1}) in DMF, whereas the low-energy absorption band at λ > 390 nm displays similar solvatochromism from 393 nm (ε = 5240 M^{-1} cm^{-1}) in CH_2Cl_2 to 403 nm (ε = 7750 M^- cm^{-1}) in DMF. In general, the $^1O_2$ quantum yields (Φ_Δ) of **1–7** recorded in CD_2Cl_2 show diminished value of (0.15 ± 0.03 – 0.55 ± 0.05) as compared to those in CD_3CN (0.42 ± 0.03 – 0.95 ± 0.05).

In summary, the ability of $[Pt(Thpy)(PPh_3)X]^{n+}$ and $[Pt(Thpy)(HThpy)Y]^{n+}$ complexes to generate singlet oxygen varies with the auxiliary ligand X or Y. Complex **5** with high Φ (0.95 ± 0.05) exhibited binding to DNA and protein, noticeable photocytotoxicity, and predominant cellular localization in the nucleus and mitochondria, revealing the potential for new development of target-specific photosensitizers (41). Furthermore, in acetonitrile, the calixarene derivatives **6** and **7** still produce singlet oxygen in moderate to high yield. Reports on the host-guest complex formation of calixarenes or cyclodextrins with neutral hydrophobic guests are well documented in the literature (42–44). Hence it may be possible to bind a variety of substrates to the calixarenes in complexes **6** and **7**, and subsequently react these substrates with singlet oxygen produced by the cylometalated Pt(II) moieties. Studies in this direction are in progress.

Supplementary Material

Refer to Web version on PubMed Central for supplementary material.

Acknowledgments

We are grateful for financial support from the Research Grant Council of the Hong Kong SAR, China (HKU 7030/06P), The University of Hong Kong, The Chinese Academy of Sciences–Croucher Foundation Funding Scheme For Joint Laboratories, and the National Natural Science Foundation of China/Research Grants Council Joint Research Scheme (N_HKU 752/08). Y. L., D. Z., and M. S. gratefully acknowledge support from the NIH-NIGMS SC1GM084776 and the NSF CREST program (NSF HRD-0932421).

References

1. Schaap, AP., editor. Singlet Molecular Oxygen. Vol. 5. Dowden, Hutchinson & Ross, Inc; Stroudsburg, Pennsylvania: 1976. p. 399
2. Rånby, B.; Rabek, JF., editors. Singlet Oxygen: Reactions with Organic Compounds and Polymers. John Wiley & Sons; New York: 1978.

3. Wasserman, HH.; Murray, RW. Singlet Oxygen. Wasserman, HH., editor. Vol. 40. Academic Press; New York: 1979.
4. Frimer, AA. Singlet O_2. CRC; Boca Raton, FL: 1985.
5. Clennan EL. New mechanistic and synthetic aspects of singlet oxygen chemistry. Tetrahedron. 2000; 56:9151–9179.
6. DeRosa MC, Crutchley RJ. Photosensitized singlet oxygen and its applications. Coord Chem Rev. 2002; 233–234:351–371.
7. Schweitzer C, Schmidt R. Physical mechanisms of generation and deactivation of singlet oxygen. Chem Rev. 2003; 103:1685–1757. [PubMed: 12744692]
8. Lang K, Mosinger J, Wagnerová DM. Photophysical properties of porphyrinoid sensitizers non-covalently bound to host molecules; models for photodynamic therapy. Coord Chem Rev. 2004; 248:321–350.
9. Chacon JN, Jamieson GR, Sinclair RS. Dye sensitised photo-oxidation of the methyl and phenyl esters of oleic and linoleic acids. Chem Phys Lipids. 1987; 43:81–91.
10. Navaratnam S, Hamblett I, Tonnesen HH. Photoreactivity of biologically active compounds. XVI. Formation and reactivity of free radicals in mefloquine. J Photochem Photobiol, B. 2000; 56:25–38. [PubMed: 11073313]
11. Greer A. Christopher Foote's Discovery of the role of singlet oxygen [$^1O_2$ ($^1\Delta_g$)] in photosensitized oxidation reactions. Acc Chem Res. 2006; 39:797–804. [PubMed: 17115719]
12. Montagnon T, Tofi M, Vassilikogiannakis G. Using singlet oxygen to synthesize polyoxygenated natural products from furans. Acc Chem Res. 2008; 41:1001–1011. [PubMed: 18605738]
13. Jiang G, Chen J, Huang JS, Che CM. Highly efficient oxidation of amines to imines by singlet oxygen and its application in ugi-type reactions. Org Lett. 2009; 11:4568–4571. [PubMed: 19810764]
14. Selke M, Foote CS. Reactions of organometallic complexes with singlet oxygen. photooxidation of vaska's complex. J Am Chem Soc. 1993; 115:1166–1167.
15. Selke M, Foote CS, Karney WL. Reactions of singlet oxygen with organometallic complexes. 2. Formation of a metastable rhodium-dioxygen complex. Inorg Chem. 1993; 32:5425–5426.
16. Selke M, Rosenberg L, Salvo JM, Foote CS. Reactions of singlet oxygen with organometallic compounds. 4. Photooxidation of cationic iridium(I) and rhodium(I) complexes with weakly bonded ligands. Inorg Chem. 1996; 35:4519–4522. [PubMed: 11666674]
17. Demas JN, Harris EW, McBride RP. Energy transfer from luminescent transition metal complexes to oxygen. J Am Chem Soc. 1977; 99:3547–3551.
18. Mulazzani QG, Sun H, Hoffman MZ, Ford WE, Rodgers MAJ. Quenching of the excited states of ruthenium(II)-diimine complexes by oxygen. J Phys Chem. 1994; 98:1145–1150.
19. García-Fresnadillo D, Georgiadou Y, Orellana G, Braun AM, Oliveros E. Singlet-oxygen ($^1\Delta_g$) production by rutheniurn(II) complexes containing polyazaheterocyclic ligands in methanol and in water. Helv Chem Acta. 1996; 79:1222–1238.
20. Gao R, Ho DG, Hernandez B, Selke M, Murphy D, Djurovich PI, Thompson ME. Bis-cyclometalated Ir(III) complexes as efficient singlet oxygen sensitizers. J Am Chem Soc. 2002; 124:14828–14829. [PubMed: 12475307]
21. Djurovich PI, Murphy D, Thompson ME, Hernandez B, Gao R, Hunt PL, Selke M. Cyclometalated iridium and platinum complexes as singlet oxygen photosensitizers: quantum yields, quenching rates and correlation with electronic structures. Dalton Trans. 2007:3763–3770. [PubMed: 17712442]
22. Shavaleev NM, Adams H, Best J, Edge R, Navaratnam S, Weinstein JA. Deep-red luminescence and efficient singlet oxygen generation by cyclometalated platinum(II) complexes with 8-hydroxyquinolines and quinoline-8-thiol. Inorg Chem. 2006; 45:9410–9415. [PubMed: 17083241]
23. Taylor RA, Law DJ, Sunley GJ, White AJP, Britovsek GJP. Towards photocatalytic alkane oxidation: the insertion of dioxygen into a platinum(II) methyl bond. Angew Chem Int Ed. 2009; 48:5900–5903.
24. Cheung TC, Cheung KK, Peng SM, Che CM. Photoluminescent cyclometallated diplatinum(II, II) complexes: photophysical properties and crystal structures of [$PtL(PPh_3)$]ClO_4 and [Pt_2L_2(μ-

dppm)][ClO_4]$_2$ (HL = 6-phenyl-2,2′-bipyridine, dppm= $Ph_2PCH_2PPh_2$). J Chem Soc, Dalton Trans. 1996:1645–1651.

25. Lai SW, Chan MCW, Cheung TC, Peng SM, Che CM. Probing d^8-d^8 interactions in luminescent mono- and binuclear cyclometalated platinum(II) complexes of 6-phenyl-2,2′-bipyridines. Inorg Chem. 1999; 38:4046–4055.
26. Lai SW, Che CM. Luminescent cyclometalated diimine platinum(II) complexes: Photophysical studies and applications. Top Curr Chem. 2004; 241:27–63.
27. Lu W, Mi BX, Chan MCW, Hui Z, Che CM, Zhu N, Lee ST. Light-emitting tridentate cyclometalated platinum(II) complexes containing σ-alkynyl auxiliaries: Tuning of photo- and electrophosphorescence. J Am Chem Soc. 2004; 126:4958–4971. [PubMed: 15080702]
28. Lai SW, Chan MCW, Peng SM, Che CM. Self-assembly of predesigned trimetallic macrocycles based on benzimidazole as non-linear bridging motifs: crystal structure of a luminescent platinum(II) cyclic trimer. Angew Chem Int Ed. 1999; 38:669–671.
29. Lai SW, Chan MCW, Cheung KK, Peng SM, Che CM. Syntheses of organoplatinum oligomers by employing N-donor bridges with predesigned geometry: Structural and photophysical properties of luminescent cyclometalated platinum(II) macrocycles. Organometallics. 1999; 18:3991–3997.
30. Lai SW, Chan QKW, Han J, Zhi YG, Zhu N, Che CM. Synthesis, structures and photoluminescent properties of cyclometalated platinum(II) complexes bearing upper-rim phosphinated calix[4]arenes. Organometallics. 2009; 28:34–37.
31. Siu PK-M, Ma D-L, Che C-M. Luminescent cyclometalated platinum(II) complexes with amino acid ligands for protein binding. Chem Commun. 2005:1025–1027.
32. Perrin, DD.; Armarego, WLF.; Perrin, DR. Purification of Laboratory Chemicals. 2. Pergamon; Oxford: 1980.
33. Demas JN, Crosby GA. The Measurement of Photoluminescence Quantum Yields. A Review. J Phys Chem. 1971; 75:991–1024.
34. SAINT: SAX area detector integration program, Version 7.34A. Bruker AXS, Inc; Madison, WI:
35. Sheldrick, GM. *SADABS*, Empirical Absorption Correction Program. University of Göttingen; Göttingen, Germany: 2004.
36. Sheldrick, GM. SHELX 97, Programs for Crystal Structure Analysis. University of Göttingen; Göttingen, Germany: 1997.
37. Battino R, Rettich TR, Tominaga T. The solubility of oxygen and ozone in liquids. J Phys Chem Ref Data. 1983; 12:163–178.
38. Steffen A, Tay MG, Batsanov AS, Howard JAK, Beeby A, Vuong KQ, Sun X-Z, George MW, Marder TB. 2,5-Bis(*p*-R-arylethynyl)rhodacyclopentadienes show intense fluorescence: Denying the presence of a heavy atom. Angew Chem Int Ed. 2010; 49:2349–2353.
39. Kvam PI, Puzyk MV, Cotlyr VS, Balashev KP, Songstad J. Properties of mixed-ligand cyclometalated platinum(II) complexes derived from 2-phenylpyridine and 2-(2′-thienyl)pyridine – voltammetric, absorption and emission studies. Acta Chem Scand. 1995; 49:645–652.
40. Maestri M, Sandrini D, Balzani V, Chassot L, Jolliet P, von Zelewsky A. Luminescence of ortho-metalated platinum(II) complexes. Chem Phys Lett. 1985; 122:375–379.
41. Cló E, Snyder JW, Ogilby PR, Gothelf KV. Control and selectivity of photosensitized singlet oxygen production: Challenges in complex biological systems. ChemBioChem. 2007; 8:475–481. [PubMed: 17323398]
42. Gutsche, CD. Calixarenes Revisited, Monographs in Supramolecular Chemistry. Stoddart, JF., editor. The Royal Society of Chemistry; Cambridge, U.K.: 1998.
43. Asfari, Z.; Böhmer, V.; Harrowfield, J.; Vicens, J., editors. Calixarenes 2001. Kluwer Academic; Dordrecht, The Netherlands: 2001.
44. Bellia F, La Mendola D, Pedone C, Rizzarelli E, Saviano M, Vecchio G. Selectively functionalized cyclodextrins and their metal complexes. Chem Soc Rev. 2009; 38:2756–2781. [PubMed: 19690752]

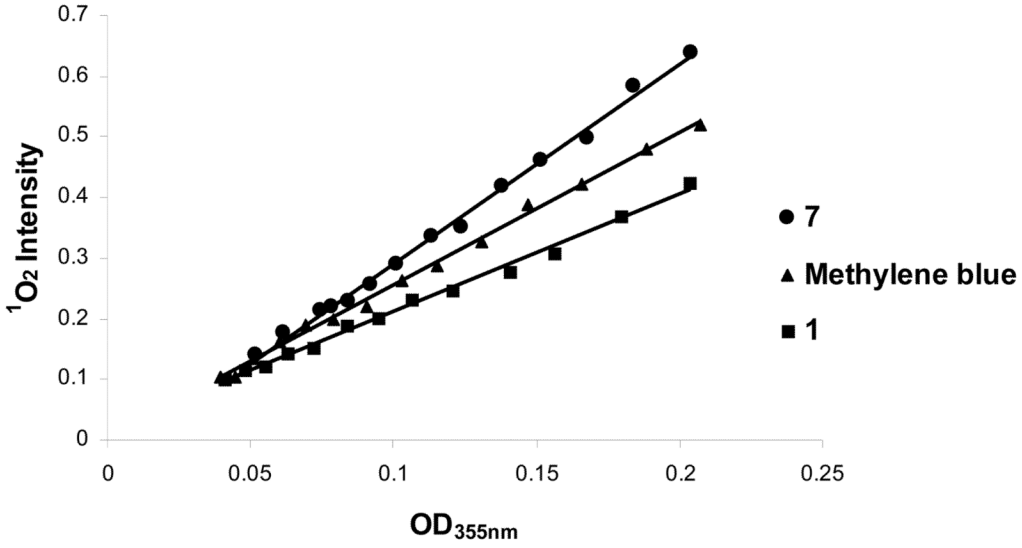

Figure 1.
A plot of $^1O_2$ emission intensity against absorption with excitation wavelength of 355 nm using sensitizers (**1** and **7**) in CD_3CN compared to that of methylene blue as a reference.

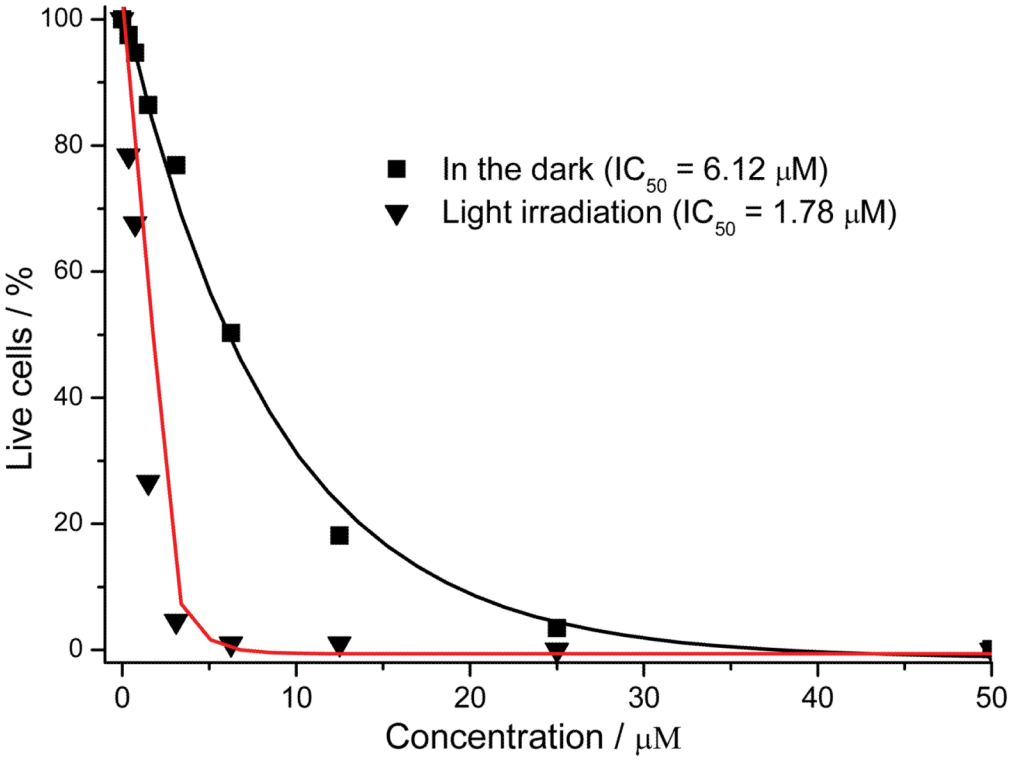

Figure 2.
Plot of percent viability of HeLa cancer cells as a function of concentration of **5** in the dark (black line) and after irradiation with visible light (red line).

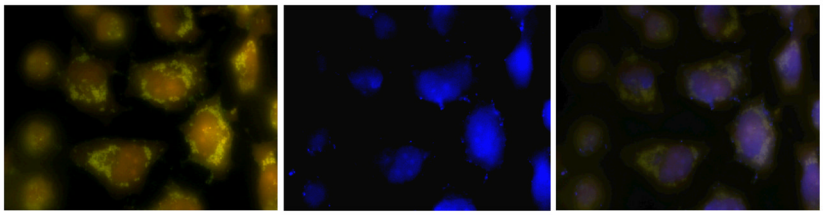

(a) (b) (c)

Figure 3.

Live cell images of HeLa cells incubated with **5** (5 μM) at 37 °C for 1 h showing (a) fluorescence emitted by **5**; (b) nucleus stained with Hoechst 33342. (c) Overlay of fluorescence images of (a) and (b).

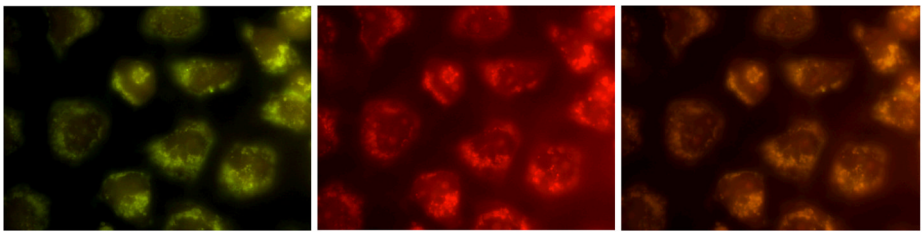

(a) (b) (c)

Figure 4.
Live cell images of HeLa cells incubated with **5** (5 μM) at 37 °C for 1 h showing (a) fluorescence emitted by **5**; (b) mitochondria stained with MitoTracker Red. (c) Overlay of fluorescence images of (a) and (b).

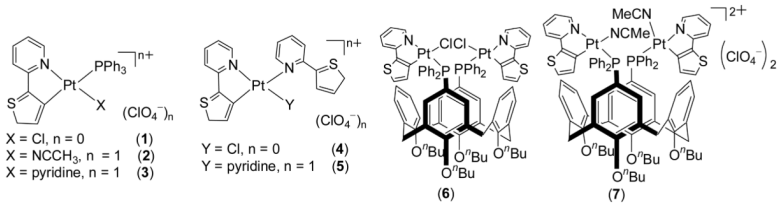

Scheme 1.
Structures of 2-(2′-thienyl)pyridyl platinum(II) complexes **1**–**7**.

Table 1

Summary of spectroscopic data: luminescence lifetime (τ), emission quantum yield (Φ), $^1O_2$ quantum yield (Φ_Δ), and quenching rate of $^1O_2$ (k_T).

Complex	[a] τ/μs		[a] Φ (λ_{max}/nm)	[b] Φ_Δ		[c] $k_T/10^7$ $M^{-1}s^{-1}$
	N_2	Air		CD_3CN	CD_2Cl_2	
[Pt(Thpy)(PPh_3)Cl], **1**	6.8	_[d]	0.020 (558)	0.44±0.02	0.12±0.03	1.40±0.04
[Pt(Thpy)(PPh_3)CH_3CN]ClO_4, **2**	26.2	_[d]	0.17 (555)	0.75±0.04	0.27±0.02	1.26±0.05
[Pt(Thpy)(PPh_3)py]ClO_4, **3**	6.73	0.26	0.056 (556)	0.82±0.06	0.55±0.05	1.46±0.04
[Pt(Thpy)(HThpy)Cl], **4**	12.0	_[d]	0.19 (556)	0.56±0.04	0.31±0.03	3.64±0.04
[Pt(Thpy)(HThpy)py]ClO_4, **5**	24.0	0.33	0.38 (554)	0.95±0.05	0.27±0.03	5.54±0.03
[(PtThpyCl)$_2$Calix(O^{n}Bu)], **6**	1.38	_[d]	0.021 (559)	0.42±0.03	0.15±0.03	0.91±0.11[e]
[{PtThpy(CH_3CN)}$_2$Calix (O^{n}Bu)]$(ClO_4)_2$, **7**	25.2	0.35	0.20 (556)	0.81±0.06	0.26±0.02	1.69±0.02

[a] Measured in CH_3CN.

[b] Determined with 355 nm excitation using methylene blue (0.57) in CD_3CN and C_{60} (1.00) in CD_2Cl_2 as references.

[c] Measured in CD_3CN unless otherwise stated.

[d] τ < 0.1 μs.

[e] Determined in CD_2Cl_2.